Advances in Ground Improvement and Principles of Track Geomechanics for Future Railways

B. Indraratna, P. Baral, Y. Qi, T.N. Ngo, C. Rujikiatkamjorn, & F.B. Ferreira
Centre for Geomechanics and Railway Engineering (CGRE) and ARC Training Centre for Advanced Technologies in Rail Track Infrastructure (ITTC-Rail), University of Wollongong Australia, NSW 2522, Australia

ABSTRACT: The need for transport infrastructure to perform for long periods of time is best shown by the way heavy haul transport networks are expected to withstand higher speeds and heavier axle loads. Ballasted rail tracks are one of the major transport systems that cater for passenger and heavy haul freight trains, but despite this advantage, geotechnical challenges such as ballast breakage, poor drainage of soft subgrade, fouling (e.g. coal and subgrade soil), pumping of clayey subgrade, differential track settlement and track misalignment due to excessive lateral displacements increase the cost of track maintenance. This means that soft deposits and problematic subgrade must be stabilised before constructing any infrastructure to prevent unacceptable differential settlement. Several ground improvement techniques are already in use, of which Prefabricated Vertical Drains (PVDs) combined with surcharge and vacuum preloading has proven to be an efficient, cost effective and popular technique for accelerating consolidation. Moreover, energy-absorbing materials manufactured from waste tyres, such as ballast mats, under sleeper pads, rubber crumbs, and tyre cells also help to attenuate dynamic train loads and vibration. These devices not only mitigate ballast degradation and deformation, they also improve track stability and increase longevity. Recycling waste materials not only helps to solve geotechnical issues, it is also economically beneficial and environmentally sustainable.

This paper presents an overview of the theoretical, experimental and numerical developments of soft ground improvement via PVDs combined with surcharge and vacuum preloading, with applications to selected case studies. Our current knowledge of how energy-absorbing materials mitigate track deterioration induced by fast moving heavy-haul trains will therefore focus primarily on research undertaken at the University of Wollongong Australia. The factors governing the stress–strain behaviour of ballast, the strength and degradation of ballast, the ability of various geosynthetics and synthetic energy absorbing mats to minimise ballast breakage and track settlement have been analysed and will be presented. These research outcomes are expected to contribute to better design solutions by considering how energy-absorbing materials enhance track stability and reduce maintenance costs.

1 INTRODUCTION

The rapid increase in population has led to an increase in the need for infrastructure, and also the need for ground improvement techniques upon which to construct stable foundations. Of these ground improvement techniques, Prefabricated Vertical Drains (PVD) with surcharge and vacuum preloading is one of the most popular because it is an efficient and effective method. However, the efficiency of PVD with surcharge can be enhanced using vacuum preloading by applying a negative pressure along the drain to reduce the consolidation time and the surcharge height as the vacuum pressure stabilises the on ground. Therefore, instead of outward lateral deformation for PVD with surcharge, applying a vacuum leads to an inward lateral deformation which solves the boundary issues, especially when constructing in a marine boundary where excessive outward lateral deformation would increase the water turbidity and thus affects the life cycles of aquatic animals.

Ballasted rail tracks are the major infrastructure catering for public and freight transport in Australia; thus the almost 40,000 km long network offers an essential supply chain for Australian agricultural and mining industries. Obviously, if the degradation of ballast due to track substructures subjected to large cyclic stresses becomes significant, the ballast becomes fouled, less angular, and its shear strength decreases (Indraratna et al. 2011, Huang et al. 2009, Powrie et al. 2007, Zhai et al. 2004), among others.

Railway companies now emphasise high-speed train corridors and heavier freight operations in order to achieve more efficient and cost-effective services, particularly in the mining and agriculture sectors, which is why incorporating synthetic energy absorbing rubber materials such as tyre cells, rubber mats and granulated rubber into rail infrastructure has become popular in recent years. Since rubber materials have very high damping properties they are expected to absorb more of the energy generated by the cyclic and impact loading of moving trains, and thus help to reduce vibration and track degradation (Sun et al. 2018, Biabani, et al. 2016). Navaratnarajah & Indraratna (2017) found that under ballast mats would reduce ballast breakage by approximately 25-45%, vertical plastic strain by approximately 10-20%, and lateral strain by approximately 5-10%. In fact it was reported that mixing ballast with 10% granulated rubber by volume will reduce ballast degradation very efficiently (Sol-Sanchez et al. 2015). Indraratna et al. (2019) indicated that rubber mats installed above the ballast will largely reduce the impact forces produced by rail irregularities and imperfections. Moreover, since these energy absorbing materials are derived from waste tyres, they are both environmentally friendly and economically beneficial. In this paper, two novel methods of using recycled rubber materials in railways will be presented: using tyre cells to reinforce the capping layer and developing a synthetic energy absorbing layer by mixing mining waste with rubber to replace the traditional sub-ballast (capping).

2 THEORETICAL DEVELOPMENT

2.1 *Vacuum consolidation*

Kjellman (1952) first introduced the concept of vacuum preloading for vertical drains in Sweden, and very quickly after at the Tianjin port in China, Philadelphia International Airport in the, USA, the North South Expressway in Malaysia (Muar Clay), reclamation works at Singapore and Hong Kong, the Second Bangkok International Airport (SBIA) in Thailand, the Ballina Bypass, Pacific Highway (New South Wales) and the Port of Brisbane (POB), Queensland in Australia, as well as many other projects (Holtan 1965; Yan and Chu 2003; Choa 1990; Jacob et al. 1994; Bergado et al. 2002, Indraratna et al. 2005a & Chu et al. 2000). Most projects for vacuum preloading are of the membrane type, although some used the membrane less technique. In most instances the vacuum pressure varies between 70-80 kPa.

The height of traditional surcharge embankments thus becomes very high, which seems to be inappropriate when using ground improvement techniques to obtain adequate strength post consolidation settlement; this is why a combined vacuum and fill surcharge approach is preferred. In this scenario the vacuum compensates for the surcharge, which limits the amount of surcharge required. The theoretical maximum suction attainable is an atmospheric pressure of 100 kPa, which is why PVD-vacuum systems are designed to distribute the vacuum (suction) pressure to deep layers in the subsoil to increase the rate that reclaimed land and deep estuarine plains will consolidate (e.g. Indraratna et al. 2005b & Chu et al. 2000).

2.2 *Development on vacuum consolidations*

By using the law of superposition, Mohamedelhassan and Shang (2002) find that the theoretical expression can be determined by superimposing vacuum and surcharge alone based on Terzaghi's 1-D consolidation theory. This combined vacuum consolidation system (Figure 1a) may be determined by combining the surcharge alone system (Figure 1b) and the vacuum alone system (Figure 1c) separately. The average degree of consolidation for combined vacuum and surcharge preloading can then be expressed by:

$$U_{vc} = 1 - \sum_{m=0}^{\infty} \frac{2}{M} \exp^{-M^2 T_{vc}} \quad (1)$$

$$T_{vc} = c_{vc} t / H^2 \quad (2)$$

where c_{vc} is the coefficient of consolidation for combined vacuum and surcharge preloading, where T_{vc} is the time factor for combined vacuum and surcharge preloading.

Indraratna et al. (2014) showed that once a vacuum pressure is applied through PVDs in the field, the vacuum pressure decreases along the depth of drain, thus reducing its project efficiency. Experiments carried out at the University of Wollongong using a large-scale consolidometer indicate that the vacuum propagates at the topmost area immediately, but then pore water pressure transducer records a loss of vacuum pressure along the depth of drain. The distribution of suction in a PVD depends mainly on the type of PVD (its core and filter properties), and its length. However, some case studies (Bo et al. 2003 & Indraratna et al. 2005a) suggest that a suction may develop rapidly even if the PVDs are up to 30 m long if the vacuum system is properly implemented. Based on laboratory observations that include the pattern of vacuum distribution, Indraratna et al. (2004, 2005a) proposed a modified radial consolidation theory (Figure 2). These results further indicate that the efficiency of PVD depends on its magnitude and the vacuum distribution system. To quantify the loss of vacuum, a trapezoidal distribution of vacuum pressure along the length of the PVD is assumed and applied in various analytical models for radial consolidation theory.

Based on these assumptions, the average excess pore pressure ratio ($R_u = \Delta p / u_o$) of a soil cylinder for radial

drainage that incorporates vacuum preloading is given by:

$$R_u = \left(1+\frac{p_0}{u_o}\frac{(1+k_1)}{2}\right)\exp\left(-\frac{8T_h}{\mu}\right) - \frac{p_0}{u_0}\frac{(1+k_1)}{2} \quad (3)$$

and

$$\mu = \ln\left(\frac{n}{s}\right)+\left(\frac{k_h}{k_s}\right)\ln(s)-0.75+\pi z(2l-z)\frac{k_h}{q_w}\left\{1-\frac{k_h/k_s-1}{(k_h/k_s)(n/s)^2}\right\} \quad (4)$$

where l is the equivalent length of drain, p_0 refers to the vacuum applied at the top of the drain, u_0 is the initial EPWP, k_1 is the ratio between the vacuum at the top and bottom of the drain, k_h, k_s are the horizontal permeability in undisturbed and smeared zones, T_h represents time factor, $n = d_e/d_w$ (d_e is the diameter of the equivalent soil cylinder = $2r_e$ and d_w is the diameter of the drain = $2r_w$), $s = d_s/d_w$ (d_s is the diameter of the smear zone = $2r_s$ with constant permeability), z = depth and q_w = drain discharge capacity.

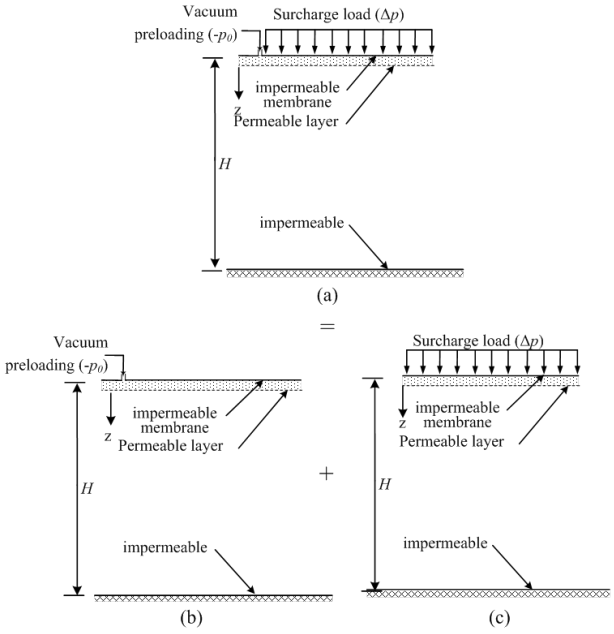

Figure 1. Schematic diagram of a vacuum preloading system (a) combined vacuum and surcharge; (b) surcharge only; and (c) vacuum only (after Mohamedelhassan and Shang 2002)

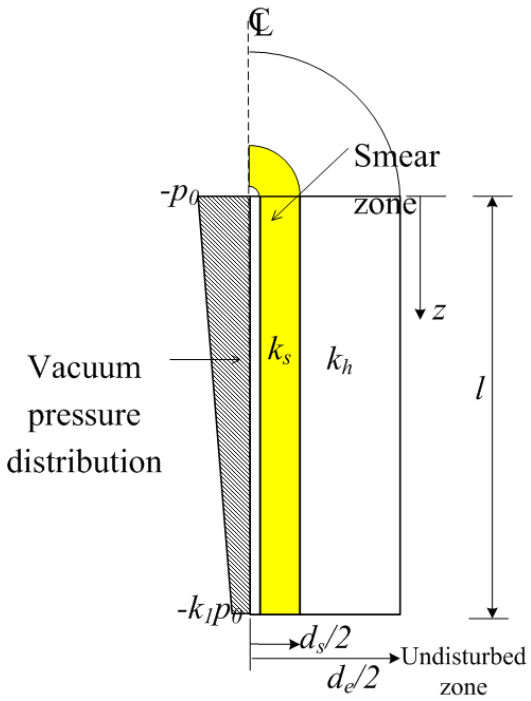

Figure 2: Vertical distribution of vacuum pressure within a PVD (after Indraratna et al., 2005a)

2.3 *Large scale consolidation with vacuum preloading*

To investigate the effect of vacuum pressure in terms of radial consolidation with undisturbed specimens, a large scale consolidometer has been formed at UOW. A corer cum consolidometer (two-in-one) built at UOW to the design by Indraratna and Redana (2000) has been used to investigate the consolidation of a large scale specimen under surcharge and vacuum preloading (Figure 3); this specimen has three main parts, the details of which are described below:

(a) A pneumatic air pressure chamber: To transfer the load to the sample during testing; and a load cell to measure the amount of load applied onto the specimens.

(b) A 350mm diameter by 700mm long cylindrical corer: Manufactured by rolling 5 mm thick steel plate and then cutting the cylinder into two halves. The custom made 345 mm diameter piston with two 5mm diameter O-rings grooves to help transfer the loads from the pneumatic air pressure chamber to the top of the specimen. The O-rings in the consolidometer help to prevent air or water leakage during the experiments. To observe the radial dissipation of pore water pressure within the specimen, two pore water pressure transducers are fitted to the bottom base plate; one in centre and another at 96.25 mm from the centre. The nature of the flow from the cell wall to the drain can be established by using the pore water pressure.

(c) The loading rig and platform: The upper part of the cylindrical corer, including the piston and air pressure chamber is attached to the loading rig, while the

lower part of the corer is attached to the base of the platform.

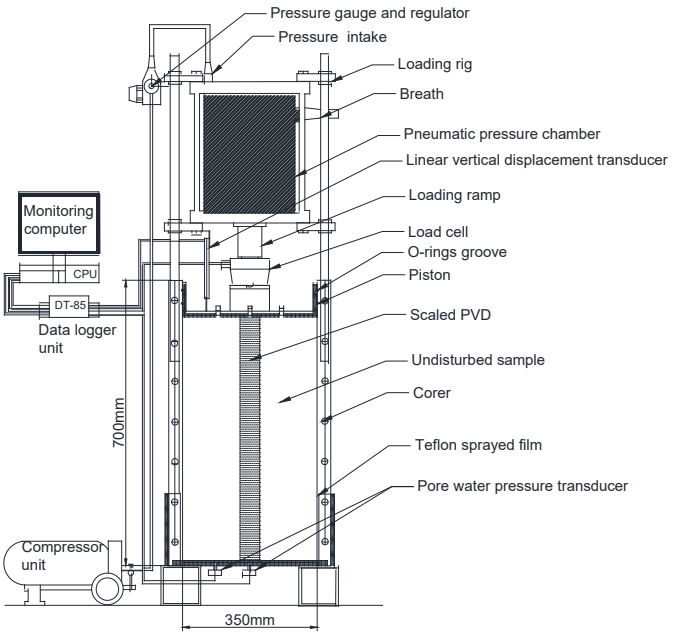

Figure 3 : Schematic diagram of large scale consolidometer (Baral et al. 2018, with kind permission from Elsevier)

A traditional type of band shaped drain measuring 100 mm by 3 mm, on the basis of an equivalent diameter and spacing in the field, has been scaled down to mimic a real field scenario, hence the model prefabricated vertical drain (PVD) is 25 mm wide by 3 mm thick (i.e. equivalent wick drain radius, r_w=7 mm). A 30mm by 5mm hollow rectangular mandrel (scaled down) is used to insert the scaled down PVD into the laboratory sample. The equivalent diameter (d_e) of this hollow rectangular mandrel is 13.8 mm. This model PVD is installed by pushing the mandrel at a constant speed down a vertical guide to the required depth inside the corer containing the undisturbed sample, and then withdrawing it immediately after reaching the base of the sample. A linear variable differential transformer (LVDT) is connected to the top of the piston to measure the vertical displacement of the sample. Two pore water pressure transducers are connected to the bottom base at different locations, and then the undisturbed sample is compressed under an axial pressure of 80 kPa. This modification also includes placing a 1.5mm diameter porous plastic sheet around the inner wall of the corer and a 1.5mm thick rubber membrane between the sample and the porous plastic sheet. A rim drain is then fitted around the piston and connected to a pressure volume controller. The rubber membrane and the wall of the corer can be separated by the inward movement of the soil due to vacuum consolidation. Based on the volume of water flowing in the gap between the wall and the rubber membrane over time, the lateral deformation of the sample can be calculated. A surcharge load of 20 kPa and a vacuum pressure 60 kPa (Vacuum Surcharge Ratio=0.75) is applied to the consolidometer.

This staged construction, as well as the settlement and PWP dissipation of an undisturbed specimen under a vacuum surcharge ratio of 0.75 is shown in Figure 4. The volumetric strain at the end of primary consolidation for a large scale specimen under given vacuum surcharge ratio is found to be 25.1 % with volume compressibility of 3.138×10^{-03} m^2/kN. Similarly, the coefficient of horizontal consolidation is found to be 4.82×10^{-03} m^2/day, which is 36 % more than the surcharge only case. This further demonstrates the efficiency of a vacuum in terms of accelerated dissipation of excess pore water pressure.

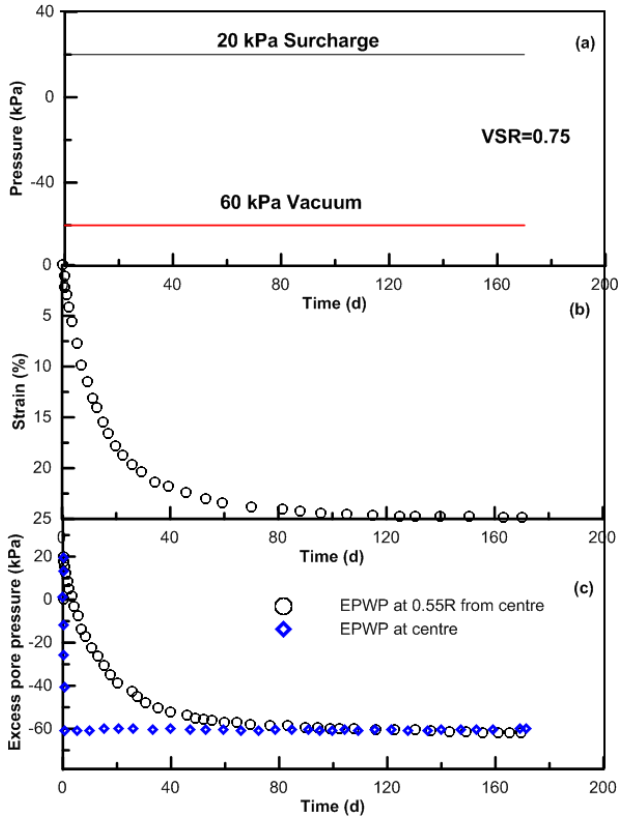

Figure 4: (a) Staged construction (b) settlement, and (c) Excess pore water pressure dissipation (Baral et al. 2008, with kind permission from Elsevier)

3 CASE HISTORY: PORT OF BRISBANE (POB)

The POB is located at the mouth of the Brisbane River at Fisherman Islands, Queensland, Australia. This site consists of 30 m thick compressible soft clays so the sub-tidal area has been reclaimed with 7 m of dredged mud capped with 2 m of sand. Since complete consolidation of these deep, soft deep clay deposits may take more than 50 years with surcharge alone, and with an associated settlement of 2.5-4 m, PVD and surcharge or PVD combined with vacuum pressure (where stability is a concern) have been trialled.

Three different contractors tested PVDs and surcharge using both membrane and membrane-less vacuum systems. Figure 5 shows the layout of the typical area to be improved.

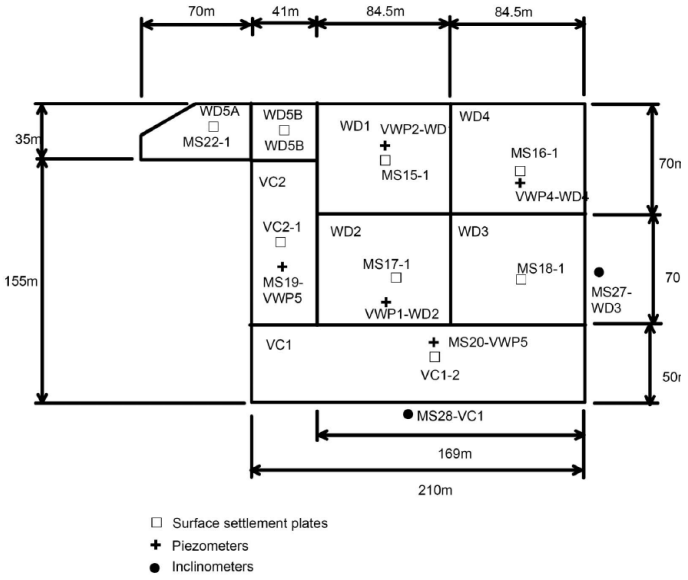

Figure 5: S3A Trial Area – Layout and detail design specifications (Indraratna et al., 2011, with permission from ASCE).

For the purpose of comparison, two sites with different loading histories and the lateral displacement normalised by the applied effective stress at two inclinometer positions (MS24 and MS34) were then compared; the results are shown in Figure 6. Note that lateral displacement occurred mostly in the shallow depths of upper Holocene clay particularly below 10 m. The data from the inclinometer, albeit limited, indicates that the membrane-less BeauDrain system (MS34) controlled the lateral displacement better than the surcharge only section (MS24). The settlement and EPWP predictions and field data for a typical settlement plate (TSP3) are shown in Figure 7; here the predicted settlement curve agrees with the field data quite well. The EPWP dissipations were more difficult to predict than settlement, but they did indicate a slower rate of dissipation in the Holocene clays, in spite of the PVDs.

With regards to stability, the incremental rate of change of the lateral displacement/settlement ratio (μ) with time is plotted in Figure 8. The rate of change of this ratio can be evaluated for relatively small time increments where a small and decreasing gradient can be considered to be stable with respect to lateral movement, whereas a continuously increasing gradient of the ratio would reflect potential lateral instability. In Figure 8, the gradient in the non-vacuum area (VC3) increased initially, possibly due to the final surcharge loading being placed quickly, while the clay was still in the early stages of consolidation. However, as the PVDs become fully active and settlement increases at a healthy rate, the gradient of μ decreases, as expected. Figure 8 shows how the vacuum pressure provides a relatively unchanging gradient of μ over time.

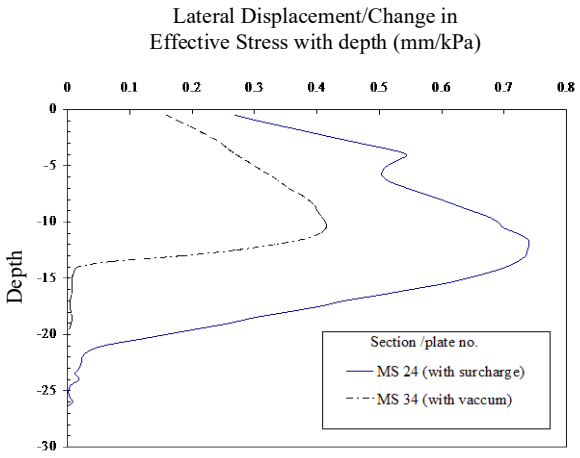

Figure 6: Comparison of lateral displacements in vacuum and non-vacuum areas (Indraratna, 2010, with permission from AGS).

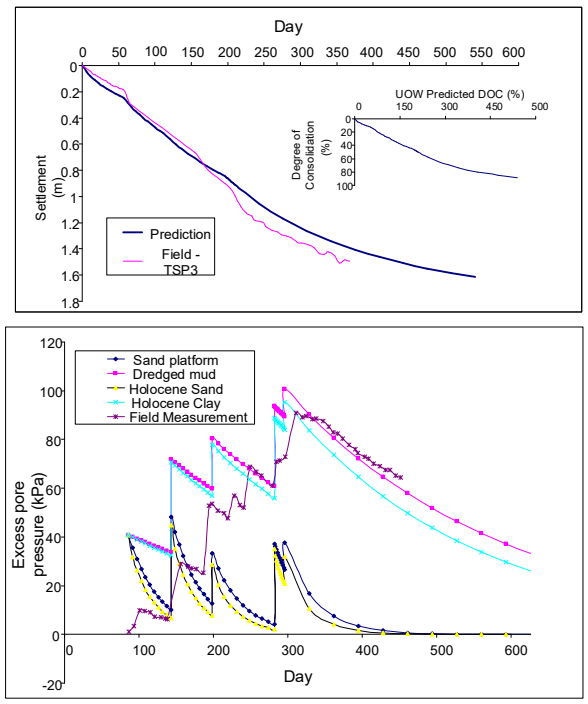

Figure 7: (a) Settlement; and (b) excess pore water pressure predictions and field data for a typical settlement plate location. (Indraratna, 2010, with permission from AGS)

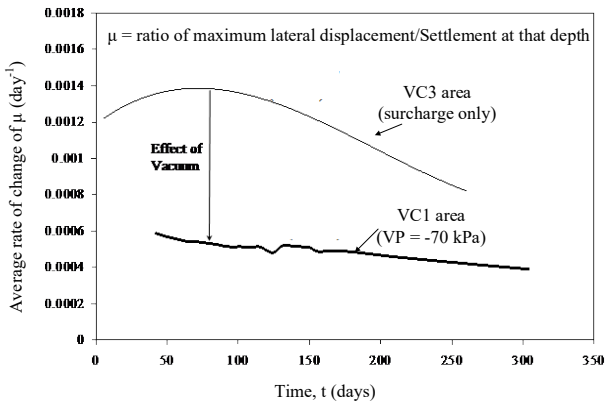

Figure 8: Rate of change of lateral displacement/settlement ratio with time (Indraratna, 2010, with permission from AGS)

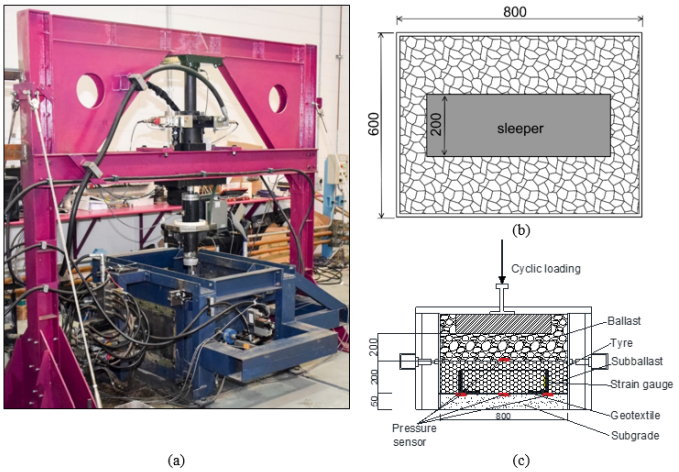

Figure 9. (a) large-scale prismoidal triaxial apparatus; (b) plan view of the prismoidal triaxial box (c) schematic illustration of the prismoidal triaxial box (modified after Indraratna et al. 2018a)

4 USE OF RUBBER INCLUSIONS IN TRACK

4.1 *Materials and test program*

An innovative method of confining the capping layer (sub-ballast) using recycled tyre cells has been proposed by Indraratna et al. (2018a), with the aim of reducing particle movement and ballast degradation while increasing the stability and resiliency of track infrastructure. Large-scale cyclic loading triaxial tests have been carried out to examine the performance of a capping layer confined by tyre cells using the large-scale process simulation primoidal apparatus (PSPTA) developed at the University of Wollongong, Australia (Fig. 9a). To simulate the field conditions of a track foundation, a simplified unit cell with area of 600×800 mm and 600 mm high is installed in the PSPTA (Figs 9b, c). The large-scale triaxial sample has 3 layers, a ballast layer, a capping layer, and a subgrade layer (Fig.1c). The ballast and capping layers are crushed basalt (latite) with particle sizes between 2.36-53 mm and 0.075-19 mm, respectively. The capping layers are confined with or without rubber tyres (one side wall removed). The bottom layer is a 50-mm thick compacted rockfill base that can simulate a typical structural fill (Indraratna et al. 2017).

The cyclic loading tests are carried out at 15 Hz to simulate a train operating at approximately 110 km/h (Indraratna et al. 2014). A maximum axial stress $\sigma'_{1cyc,max} = 385\ kPa$ and a minimum axial stress $\sigma'_{1cyc,min} = 15\ kPa$ represent the vertical stresses generated by a heavy haul train with an axle load of 40 tonnes (Jeffs & Tew 1991). Each cyclic loading test consisted of 500,000 cycles, and after each test the ballast materials were then sieved to determine the extent of degradation.

4.2 *Materials and test program*

Figure 10 shows the results of the cyclic loading test of the specimens with regards to their lateral displacement and vertical settlement. Lateral displacement of the specimen without tyre cells increases rapidly at the beginning of the test and then stabilises at around N=100,000 cycles. As expected, lateral movement of the specimen confined with tyre cell decreases dramatically because the tyre cell provides additional confinement and the particles in the infilled capping layer tend to contract more under higher with the number of loading cycles, as shown in Figure 10. Note that vertical settlement develops rapidly during the first thousands of loading cycles and then gradually stabilises after 100,000 cycles. Note also that vertical displacement of the specimen reinforced with a tyre cell reduced by almost 10-12 mm more than the specimen without a tyre cell. Overall, these test results indicate the confinement by a tyre cell reduces track settlement and lateral displacement.

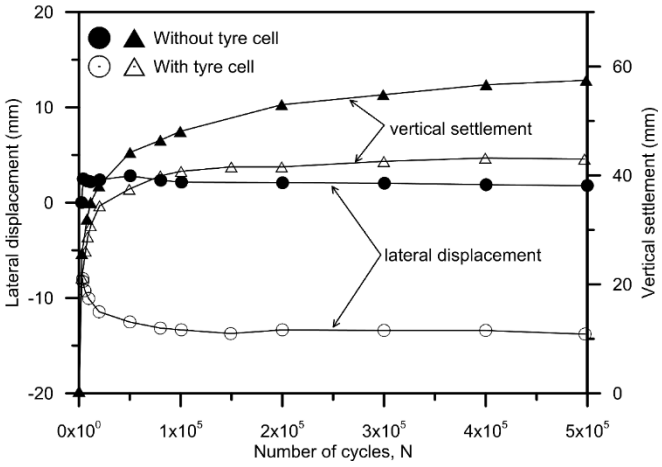

Figure 10. Lateral displacement and vertical settlement of the test specimens (modified after Indraratna et al. 2018a)

1.3 Energy dissipation analysis and ballast degradation

During loading and unloading, visco-elastic materials such as ballast exhibits hysteresis behaviour which can be evaluated by the damping ratio and dissipated energy. Figure 11a shows a typical hysteresis loop obtained during the cyclic loading tests and the corresponding equations used to calculate the damping ratio and dissipated strain energy. The damping ratio and the dissipated energy of the capping layer materials confined with and without a tyre cell are shown in Figure 11b. The tests show that confinement with a rubber tyre cell enhances the damping properties of track and increases the dissipated energy. At the beginning of the test the damping ratio and the dissipated energy decreases as the number of loading cycles increases, probably due to the high dissipation of energy by plastic sliding and particle breakage, and when there are more than 10,000 loading cycles, the damping ratio and the dissipated energy become almost constant as the granular mass stabilises and densifies. This is an important finding because this increase in the dissipation of energy can reduce the deterioration of track elements and thus reduce the frequency and cost of track maintenance.

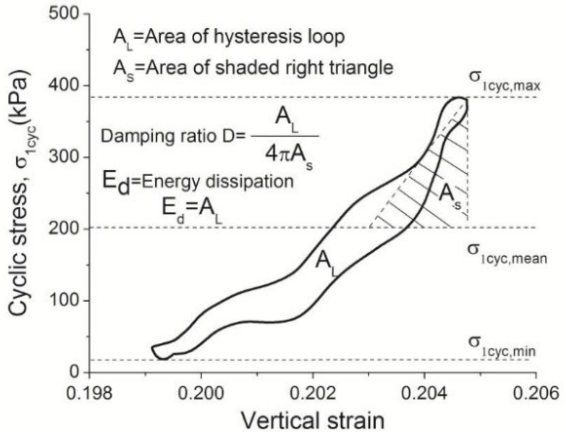

(a)

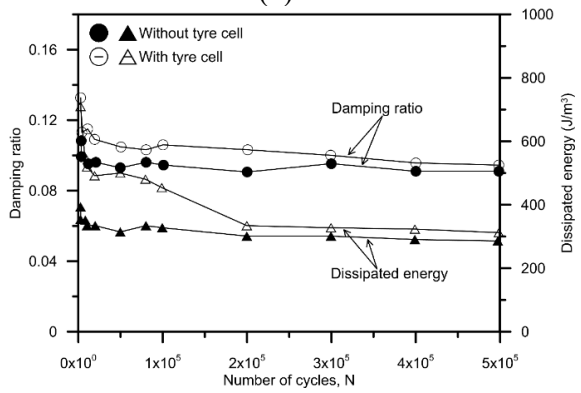

(b)

Figure 11. (a) Typical hysteresis loop showing the definition of damping ratio and energy dissipation (N=500,000); (b) variation of the damping ratio and dissipated energy with number of cycles for different test conditions (modified after Indraratna et al. 2018a)

It is reported that ballast could undergo significant degradation during long-term service due repeated impact loading (Indraratna et al. 2011), but due to their higher damping properties, the inclusion of tyre cells will reduce ballast degradation. The particle breakage of ballast is evaluated using the Ballast Breakage Index (BBI) originally proposed by Indraratna et al. (2005). The particle size distribution curves (PSD) before and after the test and the BBI of the specimens with and without a tyre cell are presented in Figure 12; note that the largest change in the size of ballast occurred in the 37.5 mm sieve. In fact the BBI of the specimen confined with a tyre cell is more than 50% less than the specimen without a tyre cell, thus indicating tyre cells definitely reduce the degradation of ballast. This result also suggests that the durability of an overall track system could be improved using rubber tyres, and thus reduce the volume of natural aggregate from the quarry.

5 A SYNTHETIC ENERGY ABSORBING LAYER FOR SUB-BALLAST USE OF RUBBER INCLUSIONS IN TRACK

5.1 *Materials and test program*

The source materials of SFS and CW are from ASMS (Australia Steel Milling Services) and Illawarra Coal Mining, respectively. The RC shredded from the waste tyres were provided by Tyre Crumbs Australia and came in three different sizes (0-2.3mm, 0.3-3mm, and 1-7 mm). The particle size distribution (PSD) curves of SFS, CW, and RC are shown in Figure 13. The dry method is used to sieve SFS and RC, whereas the wet method is used for CW because some fine particles adhered to the larger particles. SFS and CW are classified as well-graded gravel with silty-sand (GW-GM), and well-graded sand with gravel (SW) (unified soil classification system), respectively, whereas RC is referred to as granulated rubber (ASTM D6270, 2008).

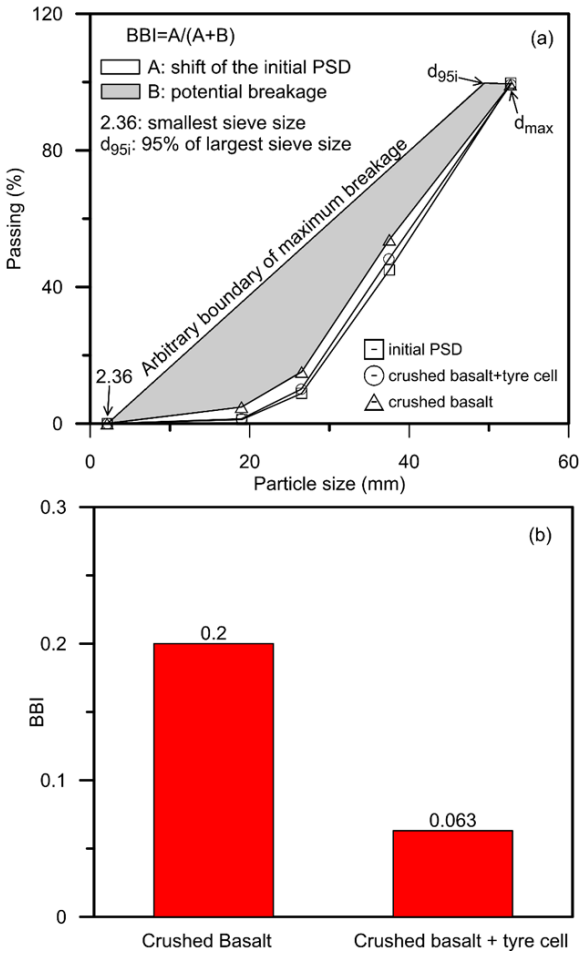

Figure 12. (a) Initial and final particle size distribution curves (PSD) of the specimens with and without tyre cell; (b) BBI of the specimens with and without tyre cell (modified after Indraratna et al. 2018a)

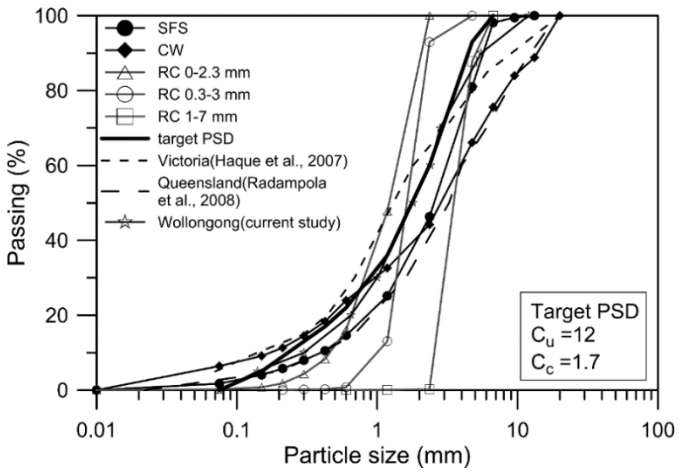

Figure 13. Particle size distribution (PSD) curves of the waste materials and selected PSD for the waste matrix (Indraratna et al. 2018b; with permission from ASCE)

To optimise the SFS+CW+RC matrix as a suitable sub-ballast material, eight parameters, i.e. gradation, permeability, peak friction angle, swell pressure, breakage index (BI), axial strain under cyclic loading, resilient modulus, and strain energy density (E) are considered based on the existing selection criteria for sub-ballast and the geotechnical properties of these three waste mixtures. These parameters are divided into three categories: (i) parameters to guarantee the functions of the capping layer (filtration, drainage and stress distribution); (ii) parameters to control the adverse geotechnical characteristics of the waste materials (volumetric expansion of SFS, particle degradation of CW, and high deformation and low strength of rubber crumbs); (iii) parameters to evaluate the energy absorbing property of the waste matrix. Comprehensive laboratory tests such as permeability tests, swell tests, and consolidated triaxial tests under both static and cyclic loading conditions have been carried out to examine these parameters.

To prevent the influence of gradation, all the waste mixtures are mixed with the same PSD (the target PSD, Fig.13) chosen by Indraratna et al. (2018b) on the basis of traditional subballast gradation in Australia. All the waste mixtures are blended by weight because this percentage is more accurate when preparing samples (Edil & Bosscher, 1994; Zheng & Kiven, 2000). The RC content (R_b, %) in the matrix is not more than 40% to prevent the sample skeleton from being totally controlled by RC (Senetakis et al., 2012; Kim & Santamarina 2008). The blending ratio of SFS:CW is set as 5:5, 7:3, and 9:1. All the specimens are blended at their optimum moisture content and then compacted to 95% of their maximum dry unit weight; the effective confining pressure σ'_3 used for the triaxial tests are 10, 40, and 70 kPa to simulate the field conditions of railway subballast. These test procedures are described in detail by Indraratna et al. (2018b).

5.2 *Stress-strain curves under static loading*

Figure 14a shows the typical stress-strain behaviour of waste mixtures with different amounts of RC and tested at $\sigma'_3 = 70\ kPa$. Note how the peak deviator stress decreases as the amount of RC increases; this is not surprising considering that rubber has very low shear strength compared to SFS and CW materials. All the specimens exhibited mainly strain softening behaviour accompanied by a contractive-dilative response. However, as the amounts of RC increases the strain softening behaviour weakens and the axial strain corresponding to the peak deviator stress also increases. This indicates that the stress-strain response changes from brittle to ductile, possibly due to an increase in the rubber-to-rubber interaction in the skeleton of the mixtures. Similar observations for mixtures of sand and rubber are also reported by Kim & Santamaria (2008). In fact, adding rubber is an advantage because the resulting higher ductility will assist the waste matrix to undergo greater plastic deformation before failure. The curves of axial strain versus volumetric strain of the waste mixtures shown in Figure 14b indicate that all the specimens are compressed and then dilate until they reach a certain axial

strain was achieved. As expected, the inclusion of more RC leads to more compression due to the high compressibility of rubber materials. The volumetric strain of SFS+CW+RC mixtures with 40% RC is almost 6% in compression.

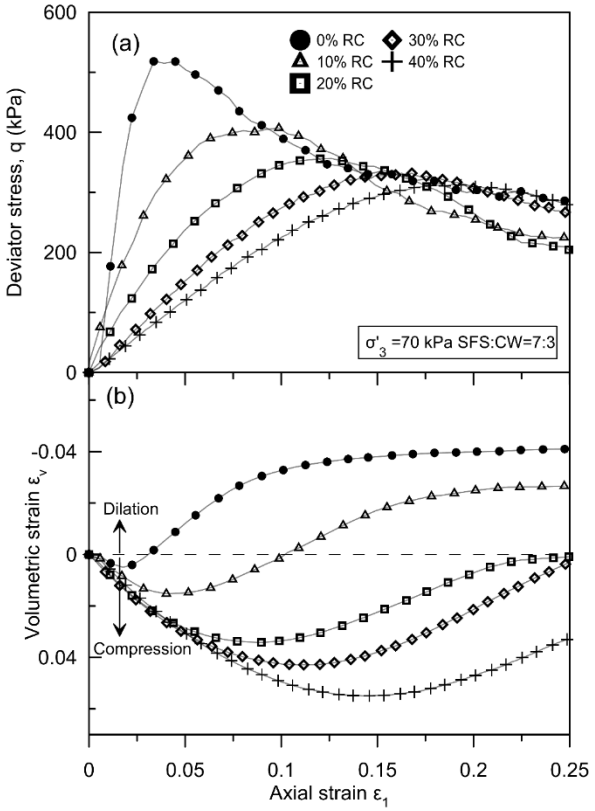

Figure 14. Stress-strain curves of the SFS+CW+RC matrix under static loading

5.3 *Strain energy density and Breakage index*

The energy absorbing property of the waste matrix is evaluated by the strain energy density which can be calculated by considering the area under the shear stress-strain curves up to failure (the peak stress state), as represented by Equation 5

$$E = \int_0^{\gamma_f} \tau d\,\gamma \qquad (5)$$

Figure 15a describes the strain energy density of the waste matrix as well as the traditional sub-ballast. Note that the strain energy density of traditional sub-ballast is similar to the waste matrix without RC, but when RC is added to the waste matrix ($R_b \geq 10\%$), the dramatic increase in the strain energy density indicates that the addition of rubber could improve the energy absorbing property of the waste matrix. Moreover, when R_b exceeds 10%, the increase in the strain energy density is marginal so 10% RC is enough to increase the energy absorbing capacity of the waste mixtures.

The breakage index (BI) is another parameter that can reflect the energy absorbing property of the waste matrix. Figure 15b shows the BI value of the waste mixtures, and as expected, the inclusion of RC could reduce the particle degradation of the waste matrix quite significantly. In fact, when $R_b \geq 30\%$, the particle breakage of SFS+CW+RC mixtures is negligible. It is assumed that if the total energy induced by the moving axle loads is a specific amount (kinetic energy), then by increasing the energy absorbing capacity of the subballast layer the energy transmitted to the ballast layer and substructure can be reduced, hence less ballast degradation is expected to occur.

5.4 *The optimum mixture*

The optimum mixture of subballast is determined by obtaining the optimal SFS:CW and the optimal amount of RC. The permeability, energy-absorbing properties and particle degradation characteristics of all the blended mixtures with $R_b \geq 10$ % and SFS:CW≥5:5 are better than traditional sub-ballast (Indraratna et al. 2018b), but a larger amount of SFS increases the volumetric expansion, however, the higher the proportion of CW, the lower the shear strength, i.e., the blending ratio of SFS:CW is the main factor governing the shear strength and the swell potential of the matrix. Therefore, the optimal ratio of SFS:CW is determined based on the test results of the swell pressure (P_{swell}) and peak friction angle ($\emptyset'_{peak}$) of a waste matrix with 10% RC (Fig. 16). To ensure that the optimum mixture has enough shear strength but less swell pressure than the typical loads applied to the capping layer, the waste mixtures are expected to satisfy $\emptyset'_{peak} \geq 49°$ (Indraratna et al. 2018b) and $P_{swell} < 30kPa$ (Ferreira et al. 2012), and thus the ratio of SFS:CW = 7:3 is the optimal ratio.

The optimal R_b is selected according to the test results from the breakage index, the peak friction angle, the resilient modulus, the strain energy density, swell pressure, and axial strain under cyclic loading of the waste matrix with SFS:CW=7:3 (Figs.17a-c). Figure 17a shows that only mixtures with R_b from 8∼18.5% satisfy the required range based on particle breakage (BI≤ 2%) and shear strength ($\emptyset_{peak} \geq 49°$), while Figure 17b shows that only mixtures with R_b from 2∼18% satisfy the required range of axial strain under cyclic loading (≤ 2%) and swell pressure ($P_{swell} < 30kPa$). Based on the strain energy density and resilient modulus, the optimal amount of RC should less than 15% (Figure 17c), and therefore the acceptable range of rubber crumbs in the waste mixtures when all of these parameters are considered should be between 8∼15%. Note too that 10% of RC is enough to substantially improve the energy-absorbing capacity of the waste mixtures without influencing the axial displacement and associated shear strength under static and cyclic loading conditions. In this context, an RC of 10% is the optimum amount and thus the

optimum mixture could be SFS63+CW27+RC10 (SFS:CW=7:3, and 10% RC).

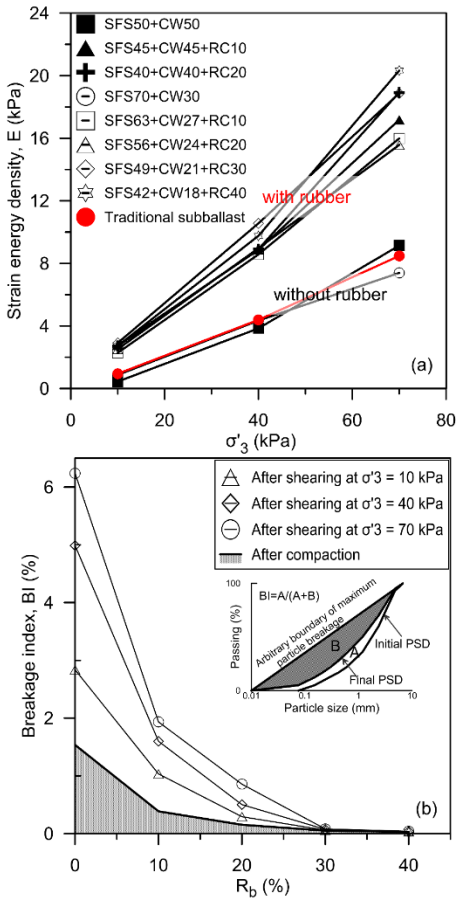

Figure 15. Test results for SFS+CW+RC matrix (modified after Indraratna et al. 2018c): (a) strain energy density varying with effective confining pressure; (b) breakage index varying with RC content

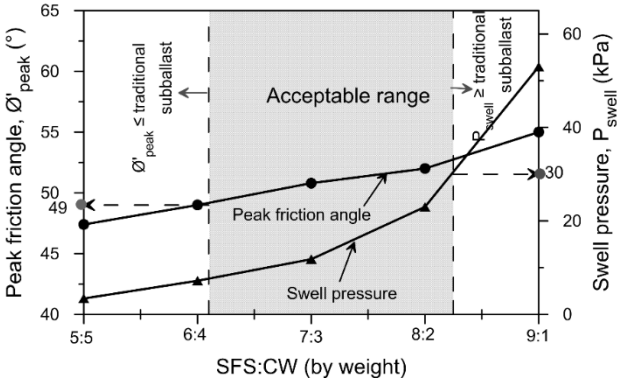

Figure 16. Optimising the blending ratio of SFS:CW (Indraratna et al. 2018b; with permission from ASCE)

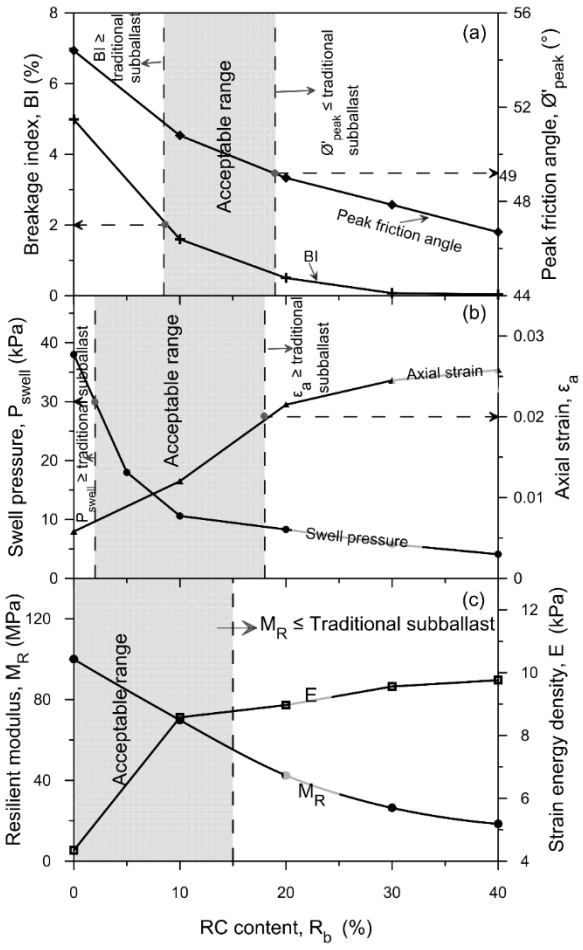

Figure 17. Optimising the RC content (Indraratna et al. 2018b and Qi et al. 2018b; with permission from ASCE)

6 BALLAST BEHAVIOUR UNDER DYNAMIC IMPACT LOADS

The ballast layer is an important part of conventional track foundations but under repeated wheel loads the aggregates tend to break and spread laterally and adversely affect the safety and efficiency of railway tracks. Further degradation may arise from dynamic impact forces created by discontinuities in the wheels or rails such as wheel flats, rail corrugations, and dipped joints, as well as abrupt variations in the stiffness of track foundations that generally occur at transition points, tunnels, road crossings and bridge approaches (Nimbalkar et al. 2012, Ferreira & Indraratna 2017, Ngo et al. 2018). A high-capacity impact test device has been used in this study to examine the rate of permanent strain accumulation and the breakage of ballast particles under repeated impact loads, and different types of synthetic inclusions such as geogrids and rubber sheets manufactured from waste tyres have also been tested; the results clearly indicate that these artificial inclusions minimise the impact-induced damage of ballast under typical field conditions.

6.1 *Test method*

The large drop-weight test facility (Fig. 18a) developed at UOW during previous research activities (Kaewunruen & Remennikov 2010) has been used to investigate the response of ballast under impact loads and also qualify the ability of geogrids and rubber mats to attenuate the damage. Test samples consisting of a 300 mm thick layer of ballast layer with an underlying 150mm thick layer of subballast were compacted inside a 300 mm diameter rubber membrane (Figs. 18b, c) with an electric vibratory hammer. A polypropylene biaxial geogrid (GGR) with 31 mm square apertures and a set of three, 10 mm thick rubber sheets were placed inside the test sample at various locations. During the test, a drop hammer (590 kg in mass) is released from a selected height to produce dynamic forces similar to those induced by typical wheel imperfections in the field (Indraratna et al. 2010). A dynamic load cell attached to the hammer records the transient impact forces generated during each blow. The incremental vertical and lateral plastic strains of the test sample were measured manually after twelve impact loads, and showed that the ballast strains to be almost negligible. The degradation of the ballast particles was then assessed using the Ballast Breakage Index (BBI) proposed by Indraratna et al. (2005). A more comprehensive description of the experimental procedures can be found elsewhere (Ferreira & Indraratna 2017, Indraratna et al. 2018c).

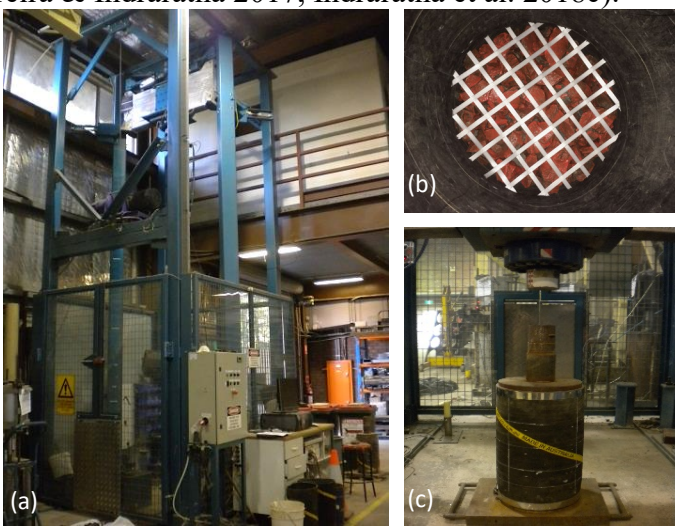

Figure 18. a) Impact test rig; b) geogrid placed within ballast during test specimen preparation; c) test specimen ready for testing.

6.2 *Test results*

Figure 19a shows the typical transient impact force-time histories recorded during the tests carried out on samples of unreinforced and reinforced ballast. The multiple peaks which occur immediately after impact represent a quasi-instantaneous reaction by the specimen to the shock, that are usually called P_1 forces (Jenkins et al. 1974); these high frequency peaks are usually followed by a smaller magnitude peak of longer duration (P_2 force). While the effects of P_1 forces are mostly filtered out by the load assembly (Frederick & Round 1985), the P_2 forces are associated with the mechanical resistance of ballast towards the dynamic impact which causes a large compression; this is why the P_2 forces cause most deterioration of track substructure (e.g. Bona 2005, Rochard & Schmid 2004) and should therefore be controlled in order to ensure track safety (British Rail Safety and Standards Board 1995).

Figure 19b shows how the P_2 forces increased with the number of successive as the ballast layer became denser. This denser granular assembly has a higher inertial resistance which then increases P_2 forces. This result suggests that the impact forces acting on a newly laid track may be lower than those on a track used more frequently where the ballast is in a denser state. Figure 19b also shows that the magnitude of the impact forces can be attenuated by placing rubber sheets above the ballast (i.e. under the sleeper pads); this is associated with the damping characteristics of this material.

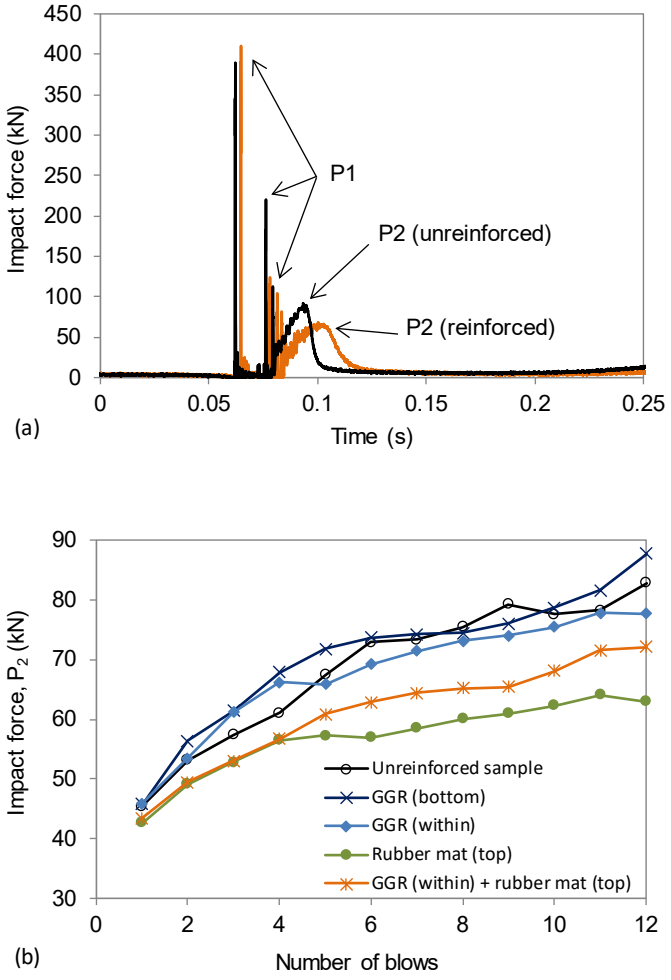

Figure 19. a) Impact force-time histories recorded in the last (12th) blow for unreinforced and reinforced ballast samples; b) variation of impact force P2 with number of blows

Figure 20 shows how the axial and radial deformation of the ballast layer accumulates due to repeated impact blows on those specimens with and without artificial inclusions. The rate of strain is more pronounced after the first blows due to the significant

reorientation and breakage of aggregates but this did tend to stabilise during subsequent impacts. However, the reinforcement elements in the test sample significantly reduced any permanent deformation; for example, a geogrid placed within the ballast mass (i.e. 100 mm above the subballast-ballast interface), attenuates the radial strains by 25%, unlike the unreinforced sample. Geogrids also restrain the lateral movement of ballast through the particle-geogrid interlock; this enhances the stability of the granular assembly and leads to a more uniform distribution of internal loads. Figure 20 also shows that the rubber mats placed above the load-bearing ballast and a geogrid sheet placed within the granular assembly further reduced the accumulation of permanent strains, leading to optimised ballast performance.

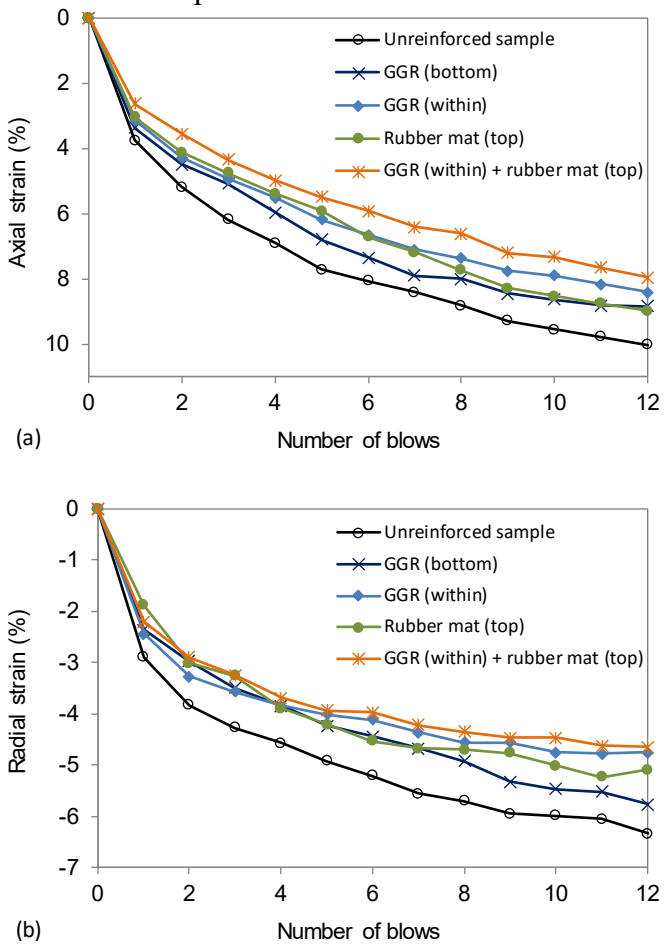

Figure 20. Effect of artificial inclusions on the permanent deformation behaviour of ballast: (a) axial strains; (b) radial strains

Table 1 lists the estimated values of BBI for the ballast samples with and without synthetic inclusions. These values range from 0.093 to 0.150, so the highest value (i.e. highest degree of breakage) corresponds to the unreinforced ballast sample. A particularly high reduction of BBI (35%) occurred when rubber mats were placed on the top of the ballast layer, thus signifying how rubber inclusions reduce and limit the extent of breakage due to impacting loads. These findings will deliver significant cost savings associated with rail track maintenance, as well as having important environmental benefits due to the re- use of scrap rubber tyres.

Table 1. Ballast breakage index for different test conditions.

Test	BBI
Unreinforced sample	0.150
GGR (bottom)	0.141
GGR (within)	0.130
Rubber mat (top)	0.097
GGR (within) + shock mat (top)	0.093

7 DISCRETE ELEMENT MODELLING OF BALLASTED RAIL TRACK

The discrete element method (DEM) introduced by Cundall and Strack (1979) is widely used to study the behaviour of granular materials. DEM is often used to model ballast because it captures the discrete nature of a granular assembly that consists of a collection of arbitrarily shaped discrete particles under quasi-static and dynamic conditions (McDowell et al. 2006, O'Sullivan *et al.* 2008, Tutumluer at al. 2012, Ngo *et al.* 2017, Indraratna et al. 2014). Particle motion is determined using Newton's second law while the interaction between particles is determined using Newton's second law of contact laws. At a given time, the force vector $\vec{F}$ that represents the interaction between the two particles is resolved into normal ($\vec{F}_N$) and the shear component ($\vec{F}_T$) with respect to the contact plane:

$$\vec{F}_N = K_N U^n \tag{6}$$

$$\delta\vec{F}_T = -K_T \cdot \delta U^s \tag{7}$$

where K_N and K_T are the normal and tangential stiffness at the contacts, U^n is the normal penetration between two particles; δU^s is the incremental tangential displacement, and $\delta\vec{F}_T$ is the incremental tangential force. The resistance moment $\vec{M}_r$ *is* introduced to represent the restraint (i.e. interlocking) between the two particles A and B and is determined by:

$$\vec{M}_r = \begin{cases} K_r\vec{\omega}_r & if \quad K_r\|\vec{\omega}_r\| < \|\vec{M}_r\|_{lim} \\ \|\vec{M}_r\|_{lim}\dfrac{\vec{\omega}_r}{\|\vec{\omega}_r\|} & if\ K_r\|\vec{\omega}_r\| \geq \|\vec{M}_r\|_{lim} \end{cases} \tag{8}$$

where, $\|\vec{M}_r\|_{lim} = \eta_r\|\vec{F}_r\|\frac{R_A+R_B}{2}$;

$K_r = \gamma_r\left(\frac{R_A+R_B}{2}\right)^2$; $\vec{\omega}_r$ is a rolling angular vector that represents the relative change in orientation between two particles that is computed by adding the angular vectors of the incremental rolling, η_r is the dimensionless coefficient, and γ_r is the rolling resistance coefficient.

7.1 *Modelling irregularly-shaped ballast particles*

Ballast particles with different shapes and sizes are modelleded by clumping many spheres together to represent actual ballast gradation (Ngo *et al.* 2017), as shown in Figure 21a. The clump approach is used to generate groups of slaved particles for modelling particles with arbitrary shapes. The basic properties of a clump are its total mass m; the location of the centre of the clump mass $x_i^{[G]}$; and the moments and products of inertia I_{ii} and I_{ij}. For a clump consisting of N_p particles, each of which has mass $m^{[p]}$, a radius $R^{[p]}$, and centroid location $x_i^{[p]}$, the mass properties are defined by Itasca (2014) as:

$$m = \sum_{p=1}^{N_p} m^{[p]} \tag{9}$$

$$x_i^{[G]} = \frac{1}{m}\sum_{p=1}^{N_p} m^{[p]} x_i^{[p]} \tag{10}$$

$$I_{ii} = \sum_{p=1}^{N_p}\left\{m^{[p]}\left(x_j^{[p]} - x_j^{[G]}\right)\left(x_j^{[p]} - x_j^{[G]}\right) + \frac{2}{5}m^{[p]}R^{[p]}R^{[p]}\right\} \tag{11}$$

$$I_{ij} = \sum_{p=1}^{N_p}\left\{m^{[p]}\left(x_i^{[p]} - x_i^{[G]}\right)\left(x_j^{[p]} - x_j^{[G]}\right)\right\}; \qquad (i \neq j) \tag{12}$$

The motion of a clump is calculated by the resultant force and the moment vectors acting upon it, but since a clump has a rigid body its motion can be described in terms of the translational motion of a point in the clump and the rotational motion of the entire clump. The equation for translational motion can be expressed in vector form:

$$F_i = m(\ddot{x}_i - g_i) \tag{13}$$

where F_i is the resultant force, the sum of all externally-applied forces acting on the clump and g_i is the body force acceleration vector arising from gravity loading.

7.2 *Modelling direct shear tests for ballast in DEM*

Figure 21 shows how DEM is used to model geogrid-reinforced ballast in a direct shear test. The dimensions of the model are the same as those in the laboratory (i.e., 300 mm long x 300 mm wide x 200 mm high). Simulated ballast grains are then placed at random locations within the specified wall boundary but without overlapping. A biaxial geogrid with 40 mm × 40 mm apertures is modelled by bonding a number of small spheres together, just like the geogrids tested in the laboratory, as shown in Figure 21b. The micromechanical parameters used to model ballast, geogrid and coal fines are adopted from Ngo *et al.* (2014).

DEM simulations of direct shear tests on fresh and fouled ballast have been carried out under three normal stresses of σ_n = 27kPa, 51kPa, and 75kPa (Figs. 21c-d), with and without the inclusion of geogrid (Ngo *et al.* 2014). Figure 22 compares the shear stress-strain behaviour of geogrid-reinforced ballast from the DEM analysis and those measured experimentally. Note that the results agree reasonably well with the laboratory data carried out by (Indraratna *et al.* 2011a) for a given normal stress and level of fouling. The strain softening behaviour of ballast and volumetric dilation evident in all the simulations show that the higher the normal stress (σ_n), the greater the shear strength and the smaller the dilation (Indraratna et al. 2016). The ability of geogrid reinforcement to increase the shear strength of fresh and fouled ballast can be seen by comparing it with an assembly with unreinforced ballast; this is due to the interlocking effect between the ballast grains and geogrid.

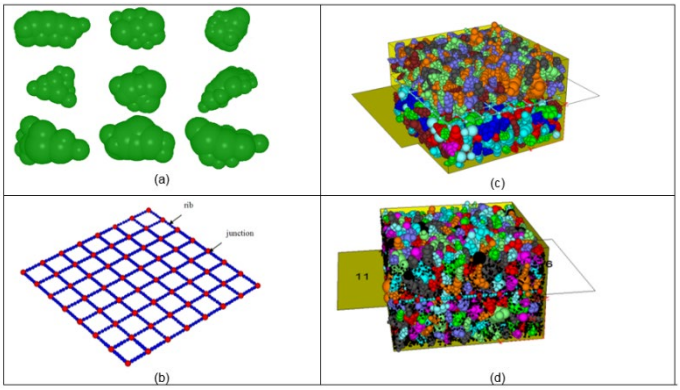

Figure 21. Simulated large-scale direct shear test for geogrid-reinforced ballast (modified after Ngo et al. 2014)

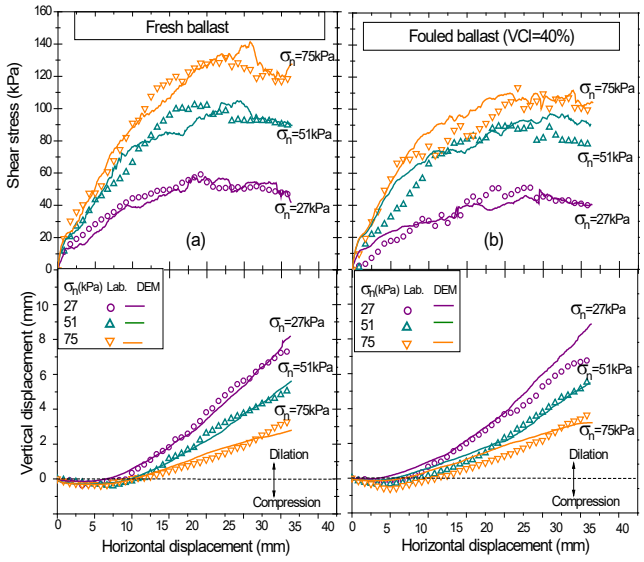

Figure 22. Comparisons of shear stress-strain of geogrid-reinforced ballast between laboratory test and DEM: (a) fresh ballast; and (b) fouled ballast (modified after Ngo et al. 2014)

8 CONCLUSIONS

In large reclamation areas as well as ground improvement projects, vacuum-assisted-consolidation has been successfully practiced. A vacuum will help to reduce the surcharge height and thus achieve the same ultimate settlement as the degree of consolidation. While a vacuum does eliminate a high surcharge, air leaks must be prevented in order to achieve the same performance. Vacuum consolidation is very much an ideal where lateral displacements must be strictly controlled, especially for marine boundaries (e.g. Port of Brisbane) where environmental and aquatic regulations are strict, to prevent water turbidity. As well as reclamation areas and road embankments, PVDs will also help to stabilise rail tracks in coastal areas with a high percentage of clayey subgrades. It has previously been shown that short PVDs can be used even under rail tracks to improve stability by dissipating excess cyclic pore pressure and curtailing lateral displacement.

Tyre cells and rubber crumbs were introduced in this paper to improve durability and reduce the degradation of track. Large-scale prismoidal triaxial tests were also carried out to investigate the performance of a capping layer reinforced with tyre cells. The test results indicate that tyre cells infilled with traditional capping layer materials can provide considerable lateral confinement and reduce the vertical settlement of a track by approximately 10-12 mm compared to the sample without tyre cells. Moreover, tyre cells can significantly reduce ballast degradation by more than half. A synthetic energy absorbing layer has been developed by mixing steel furnace slag, coal wash and rubber crumbs. Laboratory tests show convincingly that rubber crumbs will reduce particle breakage and improve the energy absorbing capacity of the waste matrix. The waste matrix was optimised by considering eight parameters, i.e. gradation, permeability, peak friction angle, swell pressure, breakage index, axial strain under cyclic loading, the resilient modulus, and the strain energy density. The resulting optimal waste matrix (SFS:CW=7:3, 10% RC) has a higher energy absorbing capacity and permeability than traditional sub-ballast materials, as well as acceptable shear strength and deformation.

The influence of geogrids and resilient rubber sheets on the mechanical response of ballast under impact loading conditions was analysed through a series of laboratory impact tests. These tests revealed that geogrid reinforcement helps to control the permanent deformation of a ballast layer due to the aggregate-geogrid interlock mechanism which improves the stability of the granular assembly and leads to a more uniform distribution of internal loads. Moreover, rubber mats reduce the magnitude of the impact forces and the extent of ballast crushing, and therefore the application of geogrids and rubber mats (i.e. under sleeper pads) within a track foundation can be an innovative and effective method of optimising track performance under high dynamic impact loads.

A series of DEM simulations were implemented for fresh and coal-fouled ballast (VCI=40%) with and without the inclusion of geogrids. Irregularly-shaped aggregates were modelled in DEM by connecting many balls together in approximate sizes and positions. The shear stress-strain responses predicted by the DEM model for fresh and fouled ballast matched reasonably well with those measured experimentally, proving that the detailed DEM model was able to simulate the stress-strain responses of ballast. There is no doubt that improved geogrid-ballast interaction, increased confinement of the capping layer by the use of rubber tyres, and the use of absorbent rubber products, particularly on harder subgrades, will lead to more resilient tracks with increased stability and longevity, a result that has significant implications for track maintenance costs.

9 ACKNOWLEDGMENTS

This research was carried out by the Australian Research Council Industrial Transformation Training Centre for Advanced Technologies in Rail Track Infrastructure (IC170100006) and funded by the Australian Government. The authors also wish to thank the financial support from the Rail Manufacturing Cooperative Research Centre (funded jointly by participating rail organisations and the Australian Federal Government's Business Cooperative Research Centre Program), with subsequent support from industry partners including the Australasian Centre for Rail Innovation, TSA (Project R2.5.1), Global Synthetics Pty Ltd, Naue GmbH & Co. KG and Foundation Specialists Group through (Project R2.5.2). Some results reported in this paper have been the result of numerous successful projects partially funded by the ARC and three consecutive Cooperative Research Centres (CRC) in the area of railway infrastructure and ground improvements. A significant portion of the contents has already been discussed in past issues of the ASCE International Journal of Geomechanics, Journal of Geotechnical and Geoenvironmental Engineering, Computers and Geotechnics, ASCE Journal of Materials in Civil Engineering, Transportation Geotechnics, Australian Geomechanics Society-AGS, among others; salient contents from these previous publications are reproduced here with kind permission from the respective sources. The authors are thankful to contributions from our colleague A/Prof Vinod S. Jayan, Dr Sanjay Nimbalka, Dr Ana Heitor, Dr Qideng Sun, and Jim Grant. The assistance provided by industry (ASMS, South 32, and Tire Crumb Australia) in relation to the procurement of material used in this study is gratefully acknowledged. The authors are also grateful to Alan Grant, Cameron Neilson, Duncan Best, and Richard Berndt

for their assistance during the laboratory work. The authors also thank Robert Clayton (English editor) for proofreading and professionally editing the manuscript.

10 REFERENCES

ASTM D6270, American Society for Tests and Materials 2008 (R2012), *Standard practice for use of scrap tyres in civil engineering applications,* ASTM D International, West Conshohocken, PA, USA.

Bergado, D. T., Balasubramaniam, A. S., Fannin, R. J. and Holta, R. D. 2002. Prefabricated vertical drains (PVDs) in soft Bangkok clay: a case study of the new Bangkok International Airport Project, *Canadian Geotechnical Journal*. 39: 304-315.

Biabani, M.M., Ngo, N.T. and Indraratna, B. (2016). "Performance evaluation of railway subballast stabilised with geocell based on pull-out testing." Geotextiles and Geomembranes, 44(4), pp: 579-591.

Baral P, Rujikiatkamjorn C, Indraratna B, Kelly R. 2018. Radial consolidation characterstics of soft undisturbed clay based on large specimens. Journal of Rock Mechanics and Geotechnical Engineering.

Bona, M.E. (2005). The effect of straightening and grinding of welds on track roughness. MSc Thesis, Queensland University of Technology.

British Rail Safety and Standards Board 1995. Commentary on permissible track forces for railway vehicles: Issue 1. GM/RC2513, Rail Safety and Standards Board, London.

Choa, V. 1990. Soil improvement works at Tianjin East Pier project. *Proceedings 10th Southeast Asian Geotechnical Conference, Taipei*, 1: 47-52.

Chu, J., Yan, S.W. & Yang, H. 2000. Soil improvement by the vacuum preloading method for an oil storage station. *Geotechnique* 50(6): 625-632.

Cundall, P.A. and Strack, O.D.L. (1979). "A discrete numerical model for granular assemblies." *Geotechnique,* 29(1), pp: 47-65.

Edil, T. and Bosscher, P. (1994) Engineering properties of tyre chips and soil mixtures, Geotechnical Testing Journal, 17(4), pp. 453-464.

Ferreira, F.B. & Indraratna, B. 2017. Deformation and degradation response of railway ballast under impact loading – effect of artificial inclusions. *Proceedings of the 1st International Conference on Rail Transportation, Chengdu, China*. Paper ID: 362: 1090-1101.

Frederick, C.O. & Round, D.J. 1985. Vertical Track Loading. Track Technology. London: Thomas Telford, 135-149.

Huang, H., Tutumluer, E., Hashash, Y.M.A. and Ghaboussi, J. (2009). "Discrete element modeling of aggregate behavior in fouled railroad ballast." Geotechnical Special Publication, 192, pp: 33-41.

Holtan, G.W. 1965. Vacuum stabilization of subsoil beneath runway extension at Philadelphia International Airport. Proc. of 6th ICSMFE, Montreal, 2: 61-65

Indraratna B. 2010. 2009 EH Davis Memorial Lecture: Recent advances in the application of vertical drains and vacuum preloading in soft soil stabilization. Australian Geomechanics Journal, AGS 45(2):1-43

Indraratna, B., Ngo, N.T. and Rujikiatkamjorn, C. (2011). "Behavior of geogrid-reinforced ballast under various levels of fouling." *Geotextiles and Geomembranes,* 29(3), pp: 313-322.

Indraratna, B. & Redana, I. 2000. Numerical modeling of vertical drains with smear and well resistance installed in soft clay. *Canadian Geotechnical Journal*, 37, 132-145.

Indraratna, B., Bamunawita, C., and Khabbaz, H. 2004. Numerical modeling of vacuum preloading and field applications. *Canadian Geotechechnical Journal*, 41: 1098-1110.

Indraratna, B., Rujikiatkamjorn C., and Sathananthan, I. 2005a. Analytical and numerical solutions for a single vertical drain including the effects of vacuum preloading. *Canadian Geotechnical Journal*, 42: 994-1014.

Indraratna, B., Sathananthan, I., Rujikiatkamjorn C. and Balasubramaniam, A. S. 2005b. Analytical and numerical modelling of soft soil stabilized by PVD incorporating vacuum preloading. *Int. Journal of Geomechanics, ASCE*, 5(2): 114-124.

Indraratna, B., Lackenby, J. & Christie, D. 2005. Effect of confining pressure on the degradation of ballast under cyclic loading. *Geotechnique* 55(4): 325-328.

Indraratna, B., Nimbalkar, S., Christie, D., Rujikiatkamjorn, C. & Vinod, J.S. 2010. Field assessment of the performance of a ballasted rail track with and without geosynthetics. *Journal of Geotechnical and Geoenvironmental Engineering* 136(7): 907-917.

Indraratna, B., Ferreira, F.B., Qi, Y. & Ngo, T.N. (2018c). "Application of Geo-inclusions for Sustainable Rail Infrastructure under Increased Axle Loads and Higher Speeds". *Innovative Infrastructure Solutions*, 3(69),

Indraratna, B., Lackenby, J and Christie, D. (2005). Effect of confining pressure on the degradation of ballast under cyclic loading. Geotechnique, 55(4), pp: 325-328.

Indraratna, B., Sun, Q., Ngo, N.T. and Rujikiatkamjorn, C. (2017). "Current research into ballasted rail tracks: model tests and their practical implications." *Australian Journal of Structural Engineering,* 18(3), pp: 204-220.

Indraratna, B., Ngo, N.T., Rujikiatkamjorn, C. and Vinod, J. (2014). "Behaviour of fresh and fouled railway ballast subjected to direct shear testing - a discrete element simulation." *International Journal of Geomechanics, ASCE,* 14(1), pp: 34-44.

Indraratna, B., Qi, Y.J. and Heitor, A (2018b), 'Evaluating the Properties of Mixtures of Steel Furnace Slag, Coal Wash, and Rubber Crumbs Used as Subballast', *Journal of Materials in Civil Engineering*, vol. 30, No.1, pp. 04017251.

Indraratna, B., Salim, W. and Rujikiatkamjorn, C. (2011). Advanced Rail Geotechnology - Ballasted Track, CRC Press, Taylor & Francis Group, London, UK.

Indraratna, B., Nimbalkar, S.S., Ngo, N.T. and Neville, T. (2016). "Performance improvement of rail track substructure using artificial inclusions – Experimental and numerical studies." *Transportation Geotechnics,* 8, pp: 69-85.

Indraratna, B., Sun, Q., Heitor, A. and Grant, J. (2018a). Performance of rubber tire-confined capping layer under cyclic loading for railroad conditions. Journal of Materials in Civil Engineering, 30(3), pp: 06017021.

Indraratna, B., Qi, Y., Ngo, T.N., Rujikiatkamjorn, C., Neville, T., Ferreira, F.B. and Shahkolahi, A (2019). 'Use of geogrids and recycled rubber in railroad infrastructure for enhanced performance-laboratory and computational study'. Geosciences, Special issue, vol. 9, No.1.

Jeffs, T. and Tew, G.P. (1991). A review of track design procedures: Sleepers and ballast, Railways of Australia, Melbourne, Australia.

Jenkins, H.M., Stephenson, J.E., Clayton, G.A., Moorland, J.W. & Lyon, D. 1974. The effect of track and vehicle parameters on wheel/rail vertical dynamic forces. *Railway Engineering Journal* 3(1): 2-16.

Kaewunruen, S. & Remennikov, A.M. 2010. Dynamic crack propagations in prestressed concrete sleepers in railway track systems subjected to severe impact loads. *Journal of Structural Engineering*, ASCE 136(6): 749-754.

Kim, H.K. & Santamarina, J.C. (2008) Sand-rubber mixtures (large rubber chips), Canadian Geotechnical Journal, 45, pp. 1457-1466.

McDowell, G.R., Harireche, O., Konietzky, H., Brown, S.F. and Thom, N.H. (2006). "Discrete element modelling of geogrid-reinforced aggregates." Proceedings of the ICE - Geotechnical Engineering 159(1), pp: 35-48.

Powrie, W., Yang, L.A. and Clayton, C.R.I. (2007). "Stress changes in the ground below ballasted railway track during train passage." *Proceedings of the Institution of Mechanical Engineers: Part F: Journal of Rail and Rapid Transit*, pp: 247-261.

Qi, Y.J., Indraratna, B., Heitor, A. & Vinod, J.S. (2018b) The Role of Rubber Crumbs on the Cyclic Behaviour of Steel Furnace Slag and Coal Wash Mixtures, Journal of Geotechnical and Geoenvironmental Engineering, 144(2), pp. 04017107.

Jacob, A., Thevanayagam, S. and Kavazajian, E., 1994. Vacuum-assisted consolidation of a hydraulic landfill. Vertical and Horizontal Deformations of Foundations and Embankments, Settlement, 94, College Station. *Geotechnical Special Publications No 40, ASCE*: 1249-1261.

Rochard, B.P. & Schmidt, F. 2004. Benefits of lower-mass trains for high speed rail operations. *Proceedings of the Institution of Civil Engineers - Transport* 157(1): 51-64.

Mohamedelhassan E., and Shang, J.Q. 2002. Vacuum and surcharge combined one-dimensional consolidation of clay soils, *Canadian Geotechnical Journal*, 39: 1126-1138.

Nimbalkar, S., Indraratna, B., Dash, S. & Christie, D. 2012. Improved performance of railway ballast under impact loads using shock mats. *Journal of Geotechnical and Geoenvironmental Engineering* 138(3): 281-294.

Ngo, N.T., Indraratna, B. and Rujikiatkamjorn, C. (2017). "Micromechanics-based investigation of fouled ballast using large-scale triaxial tests and discrete element modeling." Journal of Geotechnical and Geoenvironmental Engineering, 134(2), pp: 04016089.

Ngo, N.T., Indraratna, B. and Rujikiatkamjorn, C. (2014). "DEM simulation of the behaviour of geogrid stabilised ballast fouled with coal." Computers and Geotechnics, 55, pp: 224-231.

Ngo, N.T., Indraratna, B. and Rujikiatkamjorn, C. (2017). "A study of the geogrid–subballast interface via experimental evaluation and discrete element modelling." *Granular Matter,* 19(3), pp: 54: 51-16.

Ngo, N., Indraratna, B., Ferreira, F.B. & Rujikiatkamjorn, C. 2018. Improved performance of geosynthetics enhanced ballast: laboratory and numerical studies. *Proceedings of the ICE – Ground Improvement*, Special Issue on Geosynthetics 171(4): 202-222.

Yan, S. W. and J. Chu 2003. Soil improvement for a road using a vacuum preloading method. *Ground Improvement* 7(4): 165-172.

Johnson, H.L. 1965. Artistic development in autistic children. *Child Development* 65(1): 13-16.

O'Sullivan, C., Cui, L. and O'Neill, C. (2008). "Discrete element analysis of the response of granular materials during cyclic loading." *Soils and Foundations,* 48(4), pp: 511-530.

Polhill, R.M. 1982. *Crotalaria in Africa and Madagascar*. Rotterdam: Balkema.

Senetakis, K., Anastasiadis, A. and Pitilakis, K. (2012) Dynamic properties of dry sand/rubber (SRM) and gravel/rubber (GRM) mixtures in a wide range of shearing strain amplitudes, Soil Dynamics and Earthquake Engineering, 33(1), pp. 38-53.

Sol-Sanchez, M.; Thom, N.H.; Moreno-Navarro, F.; Rubio-Gamez, M.C.; and Airey, G.D. A study into the use of crumb rubber in railway ballast. *Construction and Building Materials* 2015, 75, 19-24.

Sun, Q., Indraratna, B. and Ngo, N.T. (2018). "Effect of increase in load and frequency on the resilience of railway ballast." *Géotechnique,* 0(0), pp: 1-8.

Tutumluer, E., Huang, H. and Bian, X. (2012). "Geogrid-aggregate interlock mechanism investigated through aggregate imaging-based discrete element modeling approach." *International Journal of Geomechanics,* 12(4), pp: 391-398.

Zhai, W.M., Wang, K.Y. and Lin, l.H. (2004). "Modelling and experiment of railwayballast vibrations." *Journal of Sound and Vibration,* 673–683, pp: 673–683.

Zheng, Y.F. and Kevin, S.G. (2000) Dynamic properties of granulated rubber/sand mixtures, Geotechnical Testing Journal, 23(3), pp. 338-344.